X-ray Diffraction Study of Water Confined in Mesoporous MCM-41 Materials over a Temperature Range of 223−298 K

Pavel Smirnov,[†] Toshio Yamaguchi,*[,†] Shigeharu Kittaka,[‡] Shuichi Takahara,[‡] and Yasushige Kuroda[§]

Department of Chemistry, Faculty of Science, Fukuoka University, Nanakuma, Jonan-ku, Fukuoka, 814-0180, Japan, Department of Chemistry, Faculty of Science, Okayama University of Science, 1-1 Ridaicho, Okayama 700-0005, Japan, and Department of Chemistry, Faculty of Science, Okayama University, Tsushima, Okayama 700-8530, Japan

Received: December 9, 1999; In Final Form: March 6, 2000

X-ray scattering measurements on water confined in the cylindrical pores of MCM-41 with different pore sizes C10 (diameter = 21 Å) and C14 (28 Å) have been performed over a temperature range of 223−298 K. Both samples were sealed in glass capillaries at relative water vapor pressures $p/p_0 = 0.3$ and 0.6 under monolayer and capillary-condensed adsorption conditions, respectively. The X-ray radial distribution functions showed the presence of a distorted tetrahedral-like hydrogen-bonded network of water in both pores, characterized by peaks at ∼2.8, ∼4.2, and ∼4.9 Å, with non-hydrogen-bonded H_2O-H_2O interactions at ∼3.3 Å and H_2O-Si interactions at ∼3.8 Å between water and the silica wall. With decreasing temperature, the number of the hydrogen-bonded H_2O-H_2O interactions at 2.8 Å increases, accompanied by the shifts of the 2.8 and 4.9 Å peaks to shorter distances and of the 4.2 Å peak to larger distances, for the capillary-condensed samples, showing a tendency to form more tetrahedral-like hydrogen-bonded water structure at subzero temperatures in both pores. The amount of the hydrogen-bonded water molecules is larger with less non-hydrogen-bonded H_2O molecules in the C14 pores than in the C10 ones, showing that decreasing pore size leads to increasing distortion and/or breaking-down of hydrogen bonds in adsorbed water structure. No significant structural change of water was observed for the monolayer sample with decreasing temperature.

Introduction

The structure of water confined in porous materials has attracted much attention in connection with the importance of scientific, technological, and biophysical problems. The properties of water absorbed in porous materials can change from those of bulk water because of geometrical confinement and interactions with wall surfaces. Water in micropores can be easily supercooled to a temperature of ∼223 K. Thus, it is anticipated that investigations of the structure and dynamics of water absorbed in porous materials give information about hydrogen bonds in supercooled water and a hint on nonfreezing water in living biological cells.

Numerous investigations of water in porous materials, especially porous silicas, have been performed by different methods during the past decades.[1−3] Despite these efforts under ambient conditions, there are only a few reports on the microscopic behaviors of water in micropores at undercooled temperatures.[4−6] Therefore, there are some questions that have to be solved, such as peculiarities of confined water structure and dependence of water structure on pore size and temperature. With respect to this point MCM-41 porous materials are one of the most suitable samples because they contain highly controlled cylindrical channels with very narrow pore size distribution. They are synthesized from silica gels using typical quaternary ammonium surfactants ($C_nH_{2n+1}-(CH_3)_3N^+$) with different alkyl chain lengths, which give different pore sizes (hereafter called C*n*). A generally accepted structural model for MCM-41 materials consists of a hexagonal arrangement of cylindrical pores embedded in a matrix of amorphous silica.[7,8]

^{1}H NMR measurements on water confined in MCM-41 have been made at undercooled temperatures.[9] On the basis of the observed NMR intensities, the authors found one or more pore-size-dependent transitions of water above 222 K and an additional transition below 209 K, which is independent of pore dimension. Furthermore, they estimated the thickness of the interfacial water (5.4 ± 1.0 Å) between the matrix surface and the solid ice phase formed in the pore center.

A study of freezing/melting behavior of water in MCM-41 samples with different pore sizes has been performed by X-ray diffraction.[10] The results showed that free water confined in pores with a diameter of 42 Å freezes abruptly at ∼232 K, giving cubic ice, while the water confined in the pores with a smaller diameter of 24 Å freezes very slowly at lower temperatures. It was also suggested that the interfacial water confined between the surface of the wall and the frozen phase of the water consists of randomly distributed water molecules. However, the microscopic structure of water in the pores was not obtained for lack of X-ray data at large scattering vectors s ($=4\pi \sin\theta/\lambda$, λ is the wavelength of X-rays and 2θ is the scattering angle) needed to derive the radial distribution function.

The dynamics of water molecules confined in MCM-41 was recently investigated by quasi-elastic neutron scattering in the temperature range 200−300 K.[11] For the translational diffusion,

* To whom all correspondence should be addressed. Tel: +81-92-871-6631, ext 6224. Fax: +81-92-865-6030. E-mail: yamaguch@sunsp1.sc.fukuoka-u.ac.jp.
† Fukuoka University.
‡ Okayama University of Science.
§ Okayama University.

10.1021/jp994326+ CCC: $19.00
Published on Web 05/20/2000

TABLE 1: Parameters of the MCM-41 Samples Prepared

sample	Na content/ ppm	surface area/ $m^2\ g^{-1}$	pore diameter/ Å	pore volume/ $cm^3\ g^{-1}$
C10	180	1069	21	0.496
C14	160	1300	28	0.926

water molecules in the pores are less mobile than those in bulk, and the mobility is decreased by narrowing of the pore size.

In the present study, we have measured X-ray scattering from water confined in two MCM-41 materials, C10 and C14. The first aim of this study was to investigate structural peculiarities of water absorbed under monolayer and capillary-condensed conditions in the porous materials. The second one was to study the influence of temperature and pore size on the water structure.

Experimental Section

Preparation of MCM-41 Samples. Two kinds of siliceous MCM-41 samples (C10 and C14) were prepared by the method of Beck et al.[7] using alkyltrimethylammonium bromide with alkyl chains of 10 and 14 C atoms, respectively. Hexagonal packing of the homogeneous cylinders of the MCM-41 samples was confirmed by electron microscopy and by observing four X-ray diffraction peaks. Surface area and pore analyses were made on N_2 adsorption isotherms measured at liquid N_2 temperature by the BET plot and the Dollimore and Heal method,[12] respectively. The specific surface areas and the pore diameters determined from the N_2 adsorption isotherms are listed in Table 1. Contents of Na were determined by atomic absorption spectrometry and are given in Table 1.

The stability of the pore surface against water was examined before preparing samples. According to adsorption measurements of water on the C10 and C14, first adsorption of water on the as prepared sample hydroxylates the surface. When the humidity is increased up to 100%, the sample is seriously damaged. However, if the humidity is below 80% the reproducible adsorption−desorption isotherms, i.e., hysteresis loop, were obtained during approximately four repeated adsorption measurements.

DSC measurements for water-filled C10 and C14 samples were previously made at a heating rate of 5 K min^{-1} after cooling to 130 K.[11] A broad endothermic peak due to melting of confined water was observed at 221 K for the C14 sample, while no peak appeared for the C10 sample. It means that water does not freeze in the latter over the temperature range investigated. The stability of pore structure during freezing of water was tested by repeating DSC measurements of cooling and warming of the water-filled C14 sample and was found to be acceptable for the present experiments by observing reproducible exothermic and endothermic peaks.

X-ray Diffraction Measurements. Sample was placed in glass capillaries in 2 mm diameter and dried under vacuum at 80 °C for 3 h. First, X-ray measurements of dry MCM-41 samples were performed. Then, capillary-condensed water samples were prepared with an in situ adsorption apparatus by adsorbing water on the MCM-41 at a water vapor pressure $p/p_0 = 0.8$ for 2 h and then reducing the pressure to 0.6. Monolayer water samples were prepared in a similar way, but the final relative pressure was adjusted to 0.3. Adsorption isotherms of water for the C10 samples are shown as an example in Figure 1. After adsorption of water, the open ends of capillaries were sealed by using epoxy glue to keep samples under the same conditions as prepared during X-ray measurements.

Cooling of samples was made on a specially designed cryostat of blowing temperature-controlled N_2 gas onto the capillary.

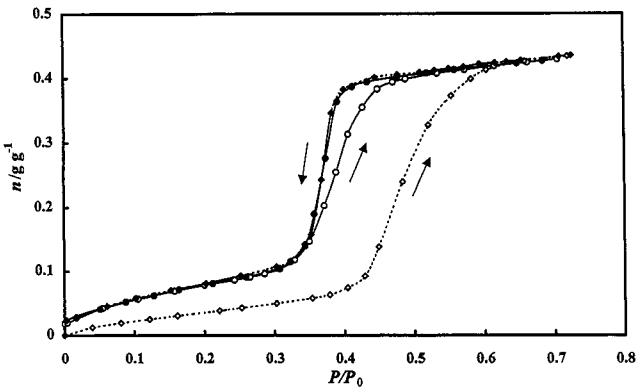

Figure 1. Adsorption isotherms of water on the MCM-41 C10 at 298 K. Key: first run, ◇ and ◆; second run, ○ and ●; open symbol, adsorption; filled symbol, desorption.

The temperature of the sample was measured with a copper−constantan thermocouple and controlled to within ±1 K.

Ice formation was visually observed on the capillary surface at temperatures below 233 K, thus no X-ray experiments at lower temperatures were made.

X-ray diffraction measurements of both dry samples and those with adsorbed water were made with a rapid liquid X-ray diffractometer DIP301 (MAC Science Co., Ltd.) using an imaging plate (IP) area detector (Fujii Film Co. Ltd) described elsewhere.[13]

The X-rays were generated at a rotary Mo anode at 50 kV and 200 mA and then monochromatized by a flat graphite crystal to obtain Mo Kα radiation (wavelength $\lambda = 0.7107$ Å). The camera length is 150 mm. A 0.9 mm collimator of double-hole type was used. The exposure time was 3 h for each sample. The effective area of IP is 200 × 400 mm, which covers the scattering angle (2θ) of 0−144° and the scattering vector s ($=4\pi \sin\theta/\lambda$) of 0−16.0 $Å^{-1}$. This wide range of scattering vector enables us to derive highly resolved radial distribution functions (RDSs) by reducing the termination error in Fourier transformation of structure functions mentioned later. After the irradiation, information on scattered intensities on IP was obtained by stimulating with a He−Ne laser beam ($\lambda = 632.8$ nm) and measuring the luminescence ($\lambda = 390$ nm) on a photomultiplier tube. Two-dimensional X-ray intensities were corrected for absorption and polarization and then integrated into one-dimensional ones.

The X-ray scattering intensities of water-adsorbed samples (wet) on MCM-41, $I_{wet}(s)$, can be represented as

$$I_{wet}(s) = I_{WW}(s) + I_{MM}(s) + I_{WM}(s) + I_C(s) \qquad (1)$$

where $I_{WW}(s)$ denotes the intensity of water adsorbed in MCM-41, $I_{MM}(s)$ that of MCM-41 itself, $I_{WM}(s)$ that of interactions between water molecules and silica walls, and $I_C(s)$ that of the cell alone.

The X-ray intensities of dry samples, $I_{dry}(s)$, can be written as

$$I_{dry}(s) = I_{MM}(s) + I_C(s) \qquad (2)$$

The experimental intensities related to the adsorbed water, $I_{WW}(s)$ and $I_{WM}(s)$, were obtained as follows.

$$I_{coh}(s) = I_{wet}(s) - I_{dry}(s) = I_{WW}(s) + I_{WM}(s) \qquad (3)$$

The experimental X-ray intensities, $I_{coh}(s)$, were corrected for multiple scattering and Compton scattering, as previously

described.[14] The structure function, $i(s)$, is given by

$$i(s) = I_{coh}(s) - \sum_i x_i f_i{}^2(s) \quad (4)$$

where $f_i(s)$ represents the atomic scattering factor of atom i corrected for the anomalous dispersion.

The radial distribution function, $D(r)$, was calculated by means of Fourier transform as

$$D(r) = 4\pi r^2 \rho_0 + 2r\pi^{-1} \int_0^{s_{max}} si(s)\, M(s) \sin(rs)\, ds \quad (5)$$

Here, ρ_0 ($=[\sum x_i f_i(0)]^2/V$) stands for the average scattering density of a sample solution in the stoichiometric volume V, and s_{max} is the maximum s value attained in the measurements ($s_{max} = 16$ Å^{-1}). A modification function $M(s)$ of the form $[\sum x_i f_i^2(0)/\sum x_i f_i^2(s)] \exp(-0.01\, s^2)$ was used.

A comparison between the experimental structure function and the theoretical one based on a model was made by a least-squares refinement procedure of minimizing an error squares sum over a selected s region from s_{min} to s_{max}

$$U = \sum_{s_{min}}^{s_{max}} s^2 \{i(s)_{exp} - i(s)_{calcd}\}^2 \quad (6)$$

The theoretical intensities, $i(s)_{calcd}$, were obtained by

$$i(s)_{calcd} = \sum_{i}\sum_{\substack{j \\ i \neq j}} x_i n_{ij} f_i(s)\, f_j(s) \sin(r_{ij}s)(r_{ij}s)^{-1} \exp(-b_{ij}s^2) - \sum_{i}\sum_{\substack{j \\ i \neq j}} x_i x_j f_i(s)\, f_j(s) 4\pi R_j^3 V^{-1} \{\sin(R_j s) - R_j s \cos(R_j s)\}(R_j s)^{-3} \exp(-B_j s^2) \quad (7)$$

The first term of the right-hand side of eq 7 is related to the short-range interactions characterized by the interatomic distance r_{ij}, the temperature factor b_{ij}, and the number of interactions n_{ij} for atom pair $i-j$. The second term arises from the interaction between a spherical hole and the continuum electron distribution beyond this discrete distance. R_i is the radius of a spherical hole around the ith atom, and B_i is the softness parameter for emergence of the continuum electron distribution.

All treatments of the X-ray diffraction data were carried out with the program KURVLR.[15]

Results and Discussion

Radial Distribution Functions (RDFs). The s-weighted experimental structure functions, $i(s)$, for both capillary-condensed and monolayer samples of C14 at different temperatures are shown by dotted lines in Figures 2 and 3, respectively, and those for capillary-condensed samples of C10 in Figure 4. The corresponding radial distribution functions are presented in Figures 5−7. For a comparison, the RDF of bulk water[13] is also illustrated in Figure 5. It should be noted that the hydrogen-bonded structure of bulk water is characterized by tetrahedral-like water−water interactions at the distances 2.85, 4.1, and 4.6 Å and non-hydrogen-bonded water−water interactions at the distance ~3.4 Å.[13,16,17]

In Figure 5, the RDFs of the C14 capillary-condensed water at 298 K have three main peaks at 2.84, 4.08, and 4.85 Å. The first peak is ascribed to the first-neighbor water−water interactions in the structure of capillary-condensed water; the peak position of 2.84 Å is not very different within experimental uncertainties (±0.02 Å) from that (2.85 Å) for bulk water. The second and third peaks, due to the second-neighbor water−water interactions, are also observed as for bulk water; however, apparently the third peak at 4.85 Å shifts by 0.2 Å from that (4.65 Å = 2.85 Å × $\sqrt{8}$/3) expected for tetrahedrally arranged water molecules in bulk water, although there is no substantial shift of the second peak at 4.08 Å. Furthermore, the intensity ratio of the first to third peaks for the C14 capillary-condensed water is much lower than that for bulk water. These findings suggest that the tetrahedral-like water structure is present in the C14 capillary-condensed water but more distorted than that found in bulk water.

When the temperature is decreased, the first peak at 2.84 Å (298 K) shifts to 2.76 Å; the second peak gradually shifts to the longer distance side, 4.08 Å (298 K), 4.15 Å (273 K), and 4.26 Å (248 K), whereas the third peak does to the shorter

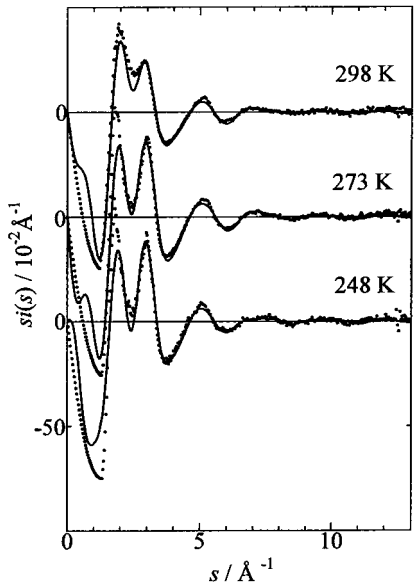

Figure 2. Structure functions $i(s)$ multiplied by s for the capillary-condensed water in MCM-41 C14. Experimental values are given by dots, and those calculated with the parameter values in Table 2 by solid lines.

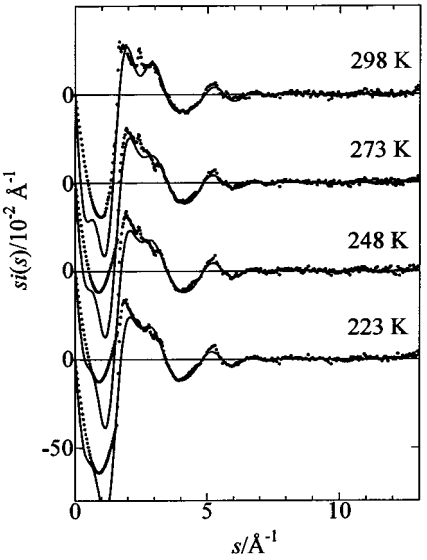

Figure 3. Structure functions $i(s)$ multiplied by s for the monolayer water adsorbed in MCM-41 C14. Experimental values are given by dots, and those calculated with the parameter values in Table 3 by solid lines.

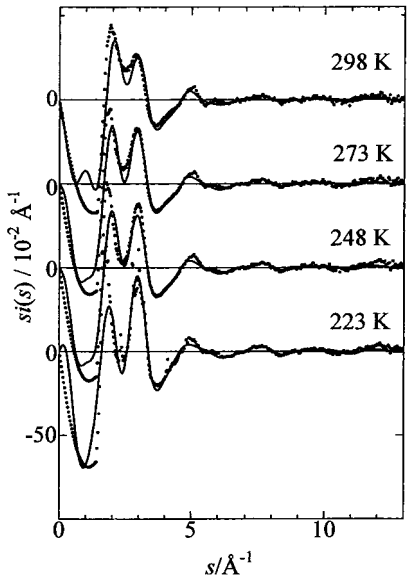

Figure 4. Structure functions $i(s)$ multiplied by s for the capillary-condensed water in MCM-41 C10. Experimental values are given by dots, and those calculated with the parameter values in Table 4 by solid lines.

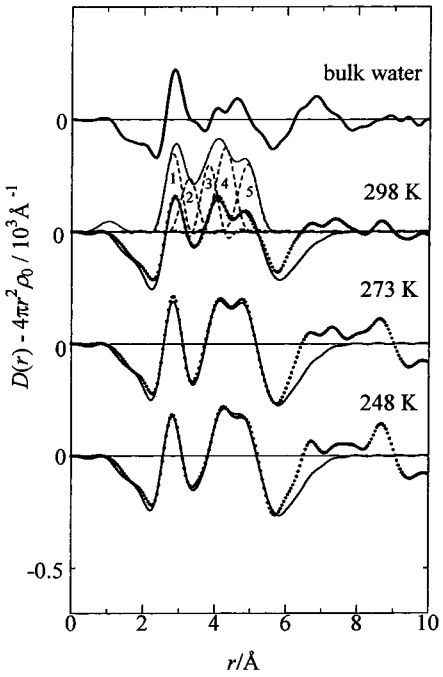

Figure 5. Radial distribution functions (RDFs) in the form of $D(r) - 4\pi r^2\rho_0$ for the capillary-condensed water adsorbed in MCM-41 C14. Experimental (dotted lines) and calculated (solid lines) values, which were obtained by Fourier transform of the values in Figure 2. Individual contributions in Table 2 are shown by dashed lines at 298 K: H_2O-H_2O at 2.81 Å (1), H_2O-H_2O at 3.34 Å (2), H_2O-Si at 3.92 Å (3), H_2O-H_2O at 4.35 Å (4), H_2O-H_2O at 4.94 Å (5). Their sum is shown by a dotted-dashed line.

distance side, 4.85 Å (298 K) and 4.76 Å (273 and 248 K). These tendencies of the peak positions suggest that in the C14 pores at subzero temperatures the distorted water−water hydrogen bonds, in particular, water in the pore center, are strengthened to form a tetrahedral-like network of water molecules, as seen in ice, although it cannot be completely built up. It should be noted that the first-neighbor and second-neighbor water−water distances in hexagonal ice are 2.78 and 4.54 Å, respectively.[18]

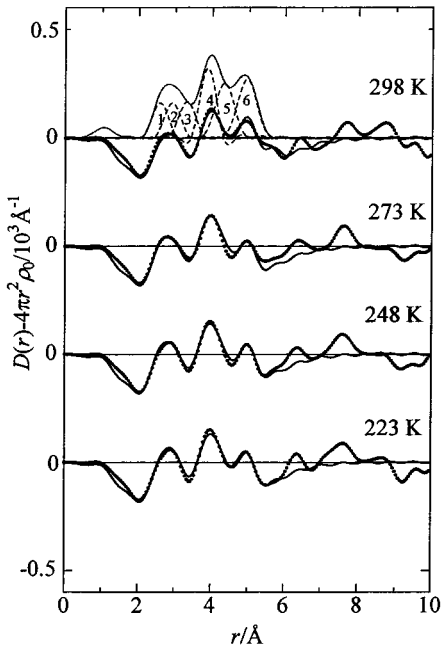

Figure 6. Radial distribution functions in the form of $D(r) - 4\pi r^2\rho_0$ for the monolayer water adsorbed in MCM41 C14. Experimental (dotted lines) and calculated (solid lines) values, which were obtained by Fourier transform of the values in Figure 3. Individual contributions in Table 3 are shown by dashed lines at 298 K: H_2O-H_2O at 2.56 Å (1), 2.90 Å (2), H_2O-H_2O at 3.30 Å (3), H_2O-Si at 3.87 Å (4), H_2O-H_2O at 4.32 Å (5), H_2O-H_2O at 4.93 Å (6). Their sum is shown by a dotted-dashed line.

It is interesting to note that the second peak at ∼4.0 Å is much more intensive for water absorbed in MCM-41 in Figure 5 than that for bulk water, in particular, for the monolayer C14 sample in Figure 6. It implies that there is another kind of interaction in the MCM-41 materials, ascribable probably to H_2O-Si interactions between water molecules and the surface of the pores, as expected from eq 3. The $Si-H_2O$ distances were expected to be ∼3.85 Å from a geometrical consideration of water molecules hydrogen-bonded to the Si−OH groups. In a neutron diffraction work on water confined in porous Vycor glass,[4] this kind of interaction was neglected. However, it has been stressed, from a neutron diffraction and neutron quasi-elastic scattering study,[6] that there are strong hydrogen bonds between water molecules and the silanol groups at the silica surface in Develosil 30 and 100 and, from a molecular dynamics simulation,[19] that the loss of water−water interactions in the immediate vicinity of the silanol surface is more than compensated in a hydrophilic case by the surface−water interactions. As seen in Figures 5 and 6, the position of the second peak shifts from 4.26 Å at 248 K for the capillary-condensed water to 4.0 Å at 248 K for the monolayer water; furthermore, the intensity of the 4.0 Å peak for the monolayer water remains similar to that for the capillary-condensed water, in contrast with those of the first and third peaks dependent on adsorbed water concentration. These results confirm that the $Si-H_2O$ interactions are present at ∼3.8 Å and become dominant for the monolayer water.

The positions and heights of the peak on the RDFs of the monolayer water in Figure 6 made much less change with temperature, showing less temperature dependence of the monolayer water structure, in contrast to those for the capillary-condensed water. It is also clearly seen in Figure 6 that the first peak becomes very broad and less intensive than that for the capillary-condensed water.

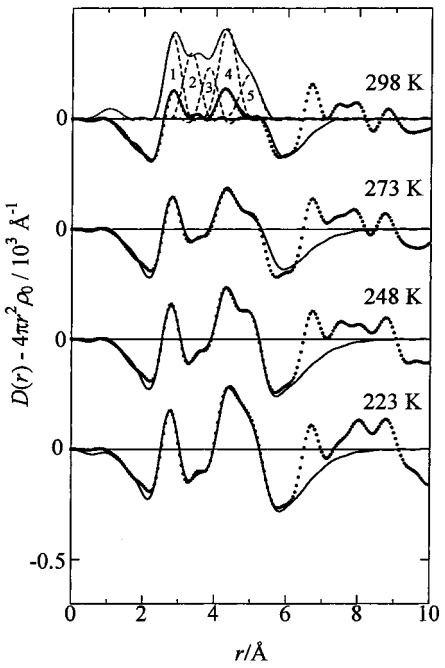

Figure 7. Radial distribution functions (RDFs) in the form of $D(r) - 4\pi r^2\rho_0$ for the capillary-condensed water adsorbed in MCM-41 C10. Experimental (dotted lines) and calculated (solid lines) values, which were obtained by Fourier transform of the values in Figure 4. Individual contributions in Table 3 are shown by dashed lines at 298 K: H_2O-H_2O at 2.78 Å (1), H_2O-H_2O at 3.33 Å (2), H_2O-Si at 3.85 Å (3), H_2O-H_2O at 4.33 Å (4), H_2O-H_2O at 4.95 Å (5). Their sum is shown by a dotted-dashed line.

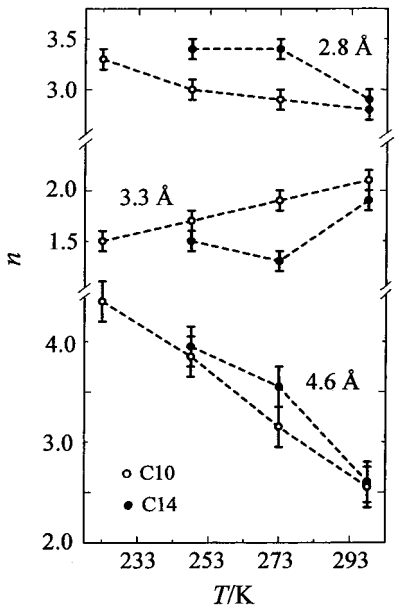

Figure 8. Coordination numbers of water molecules at different distances in the MCM-41 C10 and C14 capillary-condensed water.

The experimental peaks for the C10 capillary-condensed sample in Figure 7 were interpreted in a similar way as for the corresponding C14 sample. However, there are some differences between the RDFs of the C14 and C10 capillary-condensed water. The first and second peaks for the C10 sample are observed at 2.78 and 4.3 Å, respectively, and are almost independent of temperature; these distances are close to those found for the C14 capillary-condensed water at subzero temperatures. This finding indicates strong hydrogen bonds between the water molecules and silanol groups on the surface of MCM-41. The third peak at 5.0 Å for the capillary-condensed water is much weaker for C10 than for C14. With decreasing temperature, the second peak at 4.3 Å is gradually enhanced, showing evolution of the hydrogen-bonded network. There appears a small peak at ~3.5 Å at 298 K, ascribed probably to the interactions between non-hydrogen-bonded water molecules.[16,17] The presence of the well-separated peak at ~3.5 Å for the C10 capillary-condensed sample at 298 K indicates a significant contribution of the interactions between non-hydrogen-bonded water molecules to the water structure in the C10 pores. Intensity of this peak markedly decreases with cooling of the sample, suggesting re-forming hydrogen bonds at subzero temperatures.

Model Fitting. To analyze the interactions quantitatively the model fitting was carried out. All calculations were performed with the program NLPLSQ.[20] In subsequent analysis of the X-ray data, all the interactions discussed above were taken into account. The initial values of the distances r_{ij}, coordination numbers n_{ij}, and temperature factors b_{ij} were estimated by a trial-and-error r-space analysis where the observed RDFs were compared with theoretical peaks shapes calculated with eqs 5 and 7 until a smooth background curve was obtained. The distances, coordination numbers, and temperature factors were all allowed to vary in the first stage of the fitting procedure. However, since the temperature factors strongly correlate with the coordination numbers, as seen in eq 7, the temperature factors were fixed to the values obtained at 298 K in subsequent fittings, so that the change in coordination number with temperature would be clearly figured out.

The parameter values of optimal models are summarized in Tables 2−4. The coordination numbers seemed to be slightly overestimated, probably because of some inaccuracies in adsorption correction caused by difficulty in estimating densities of samples sealed in capillaries. Theoretical functions calculated by using the values in Tables 2−4 were plotted in Figures 2−7. The peak shapes of the individual interactions at 298 K are also shown as an example in Figures 5−7. The agreement between the experiments and the models is fairly good, except for the s region below 3 Å^{-1} in the structure functions and the r region above 6 Å in the RDFs, to which other long-range interactions not taken into account in the present analysis contribute.

The temperature dependences of the coordination numbers of water molecules are illustrated in Figures 8 and 9. As can be seen in Figure 8, the coordination number of water molecules at the distance of 2.8 Å increases with decreasing temperature for the C14 capillary-condensed sample. At the same time a mean coordination number of water molecules at 4.3 and 4.9 Å, denoted as 4.6 Å, also increases. Since both interactions are ascribed to those between water molecules in the hydrogen-bonded network of water, the results show that the hydrogen-bonded water structure is gradually enhanced in the pores with decreasing temperature.

For the monolayer C14 sample the amounts of all water−water interactions do not change significantly with decreasing temperature (Table 3 and Figure 9). A main contribution to the RDF in this case comes from bound water. From these results it can be concluded that the structure of bound water does not change significantly with cooling of sample, consistent with the fact that no peaks due to melting and crystallization of ice have been observed for the monolayer water for C14.[11]

In the case of the C10 capillary-condensed sample the trends of increase or decrease in coordination numbers are similar to those for the corresponding C14 sample. The coordination numbers of water molecules at the distances 2.8, 4.3, and 4.9 Å increase with decreasing temperature. The coordination

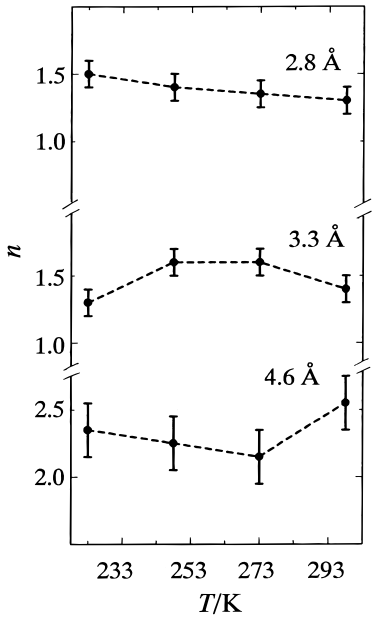

Figure 9. Coordination numbers of water molecules at different distances in the MCM-41 C14 monolayer sample.

TABLE 2: Optimized Parameter Values of the Interactions for the Capillary-Condensed Water in MCM-41 C14[a]

C14		248 K	273 K	298 K
H_2O-H_2O	*r*	2.78(2)	2.79(2)	2.81(2)
	b	0.010	0.010	0.010
	n	3.4(1)	3.4(1)	2.9(1)
H_2O-H_2O	*r*	3.33(2)	3.35(2)	3.34(2)
	b	0.012	0.012	0.012
	n	1.5(1)	1.3(1)	1.9(1)
H_2O-Si	*r*	3.90(2)	3.90(2)	3.92(2)
	b	0.015	0.015	0.015
	n	1.2(1)	1.3(1)	1.4(1)
H_2O-H_2O	*r*	4.39(2)	4.37(2)	4.35(2)
	b	0.020	0.020	0.020
	n	4.3(2)	3.7(2)	2.8(2)
H_2O-H_2O	*r*	4.90(2)	4.90(2)	4.94(2)
	b	0.023	0.023	0.023
	n	3.6(1)	3.4(1)	2.4(1)

[a] *r*, *b*, and *n* represent the interatomic distance (Å), temperature factor (Å^2), and coordination number, respectively. The values in parentheses are estimated standard deviations of the last figures. The parameters without standard deviations were fixed during the calculations. *R* and *B* values were used as 4.59 Å and 0.75 Å^2, respectively, for the oxygen atom, and 1.0 Å and 0.1 Å^2, respectively, for the hydrogen atom.

numbers at the distances 2.8, 4.3, and 4.9 Å are larger for C14 than for C10, demonstrating more hydrogen-bonded water structure inside the larger C14 pores (Table 1). The coordination numbers of the non-hydrogen-bonded water molecules at the distance of 3.3 Å decrease with cooling of both capillary-condensed samples. This result suggests that the non-hydrogen-bonded water molecules are involved in re-forming a hydrogen-bonded water structure at subzero temperatures. The amount of non-hydrogen-bonded water molecules is larger in the C10 sample than in the C14 one, showing that decreasing pore size leads to increasing non-hydrogen-bonded part in the water structure. This also illustrates that the non-hydrogen-bonded water molecules play an important role in nonfreezing of water in the C10 pores.

The amount of interaction between water molecules and the surface of the porous wall hardly changes with temperature. It is seen in Tables 2 and 3 that the amount of water−silicon interactions is larger in the C14 sample than in the C10 one because of the larger surface area of the former (Table 1).

TABLE 3: Optimized Parameter Values of the Interactions for the Monolayer Water in MCM-41 C14[a]

C14		223 K	248 K	273 K	298 K
H_2O-H_2O	*r*	2.56(2)	2.56(2)	2.56(2)	2.56(2)
	b	0.010	0. 010	0. 010	0. 010
	n	1.3(1)	1.3(1)	1.3(1)	1.3(1)
H_2O-H_2O	*r*	2.90(2)	2.88(2)	2.88(2)	2.90(2)
	b	0.010	0. 010	0. 010	0. 01
	n	1.7(1)	1.5(1)	1.4(1)	1.3(1)
H_2O-H_2O	*r*	3.30(2)	3.30(2)	3.30(2)	3.30(2)
	b	0.012	0.012	0.012	0.012
	n	1.3(1)	1.6(1)	1.6(1)	1.4(1)
H_2O-Si	*r*	3.87(2)	3.87(2)	3.87(2)	3.87(2)
	b	0.015	0.015	0.015	0.015
	n	1.5(1)	1.5(1)	1.4(1)	1.4(1)
H_2O-H_2O	*r*	4.30(2)	4.29(2)	4.31(2)	4.32(2)
	b	0.020	0.020	0.020	0.020
	n	2.5(1)	2.3(1)	2.3(1)	2.4(1)
H_2O-H_2O	*r*	4.95(2)	4.93(2)	4.89(2)	4.93(2)
	b	0.023	0.023	0.023	0.023
	n	2.2(1)	2.2(1)	2.0(1)	2.7(1)

[a] *r*, *b*, and *n* represent the interatomic distance (Å), temperature factor (Å^2), and coordination number, respectively. The values in parentheses are estimated standard deviations of the last figures. The parameters without standard deviations were fixed during the calculations. *R* and *B* values were used as 4.59 Å and 0.75 Å^2, respectively, for the oxygen atom and 1.0 Å and 0.1 Å^2, respectively, for the hydrogen atom.

As can be seen from Tables 2 and 3, the first nearest-neighbor distance in the capillary-condensed water structure is shorter for the MCM-41 samples than for bulk water. There could be two explanations about this result. The first one can be a large distortion of the water structure inside the pores, which has been noted in a neutron diffraction study for water absorbed in Vycor glass.[21] This is similar to what happens in bulk water when pressure is applied.[22] The second reason for the short hydrogen bond can be in an acidic feature of the pore surface (−Si−OH). The isoelectric point of the silanol group has been reported to be 3.0,[23] suggesting the preferable formation of H_3O^+ in water confined in the MCM-41 pores. According to a "fragmented cluster model", absorbed water can be described as a mixture of isolated monomers H_3O^+ and $H_5O_2^+$.[24] Hydration of H_3O^+ is characterized by short distances at ∼2.45 Å;[25,26] therefore, the contribution of such kinds of interactions into RDF can lead to a shift of peak position to shorter distances.

For the monolayer sample the influence of acidity should be most enhanced because the bulklike water−water interactions are negligible; as seen in Figure 6, this really occurs as the broad and less intensive first peak on the RDFs. This is also confirmed from the results in Table 3, where the first peak is described by two kinds of hydrogen bonds: the short hydrogen bonds at 2.56 Å and typical bulklike water−water interactions at 2.90 Å. The second-neighbor water−water interactions in a hydrogen-bonded water structure are represented in the model (Table 3) by two interactions at 4.3 and 4.9 Å, showing possible distortion of the water structure. The interactions between water molecules and the surface of porous wall occur at the distance ∼3.8 Å, as is also seen in the C14 and C10 capillary-condensed samples.

Conclusions

X-ray measurements on water confined in MCM-41 with varying pore sizes, C10 (diameter = 21 Å) and C14 (28 Å), at different temperatures have shown that the coordination number of water molecules at 2.8, 4.3, and 4.9 Å increases in both samples with capillary-condensed water by cooling. It proved the evolution of hydrogen-bonded structure in the adsorbed water with decreasing temperature. There is more hydrogen-

TABLE 4: Optimized Parameter Values of the Interactions for the Capillary-Condensed Water in MCM-41 C10[a]

interactions C10		Temperature 223 K	248 K	273 K	298 K
H_2O-H_2O	*r*	2.75(2)	2.76(2)	2.77(2)	2.78(2)
	b	0.010	0. 010	0. 010	0. 010
	n	3.3(1)	3.0(1)	2.9(1)	2.8(1)
H_2O-H_2O	*r*	3.33(2)	3.33(2)	3.33(2)	3.33(2)
	b	0.012	0.012	0.012	0.012
	n	1.5(1)	1.7(1)	1.9(1)	2.1(1)
H_2O-Si	*r*	3.84(2)	3.84(2)	3.85(2)	3.85(2)
	b	0.015	0.015	0.015	0.015
	n	0.8(1)	0.9(1)	0.9(1)	1.0(1)
H_2O-H_2O	*r*	4.36(2)	4.35(2)	4.34(2)	4.33(2)
	b	0.020	0.020	0.020	0.020
	n	5.1(2)	4.4(2)	3.9(2)	3.6(2)
H_2O-H_2O	*r*	4.95(2)	4.95(2)	4.96(2)	4.95(2)
	b	0.023	0.023	0.023	0.023
	n	3.7(2)	3.3(2)	2.4(2)	1.5(2)

[a] *r*, *b*, and *n* represent the interatomic distance (Å), temperature factor (Å^2), and coordination number, respectively. The values in parentheses are estimated standard deviations of the last figures. The parameters without standard deviations were fixed during the calculations. *R* and *B* values were used as 4.59 Å and 0.75 Å^2, respectively, for the oxygen atom, and 1.0 Å and 0.1 Å^2, respectively, for the hydrogen atom.

bonded water structure in the capillary-condensed C14 sample than in the C10 one, whereas the amount of non-hydrogen-bonded water molecules is larger in the latter than in the former. It shows that a decrease in porous size leads to an increase in non-hydrogen-bonded part in the water structure. It has been observed that the non-hydrogen-bonded water molecules at 3.3 Å take part in re-forming the hydrogen bonds at subzero temperatures. The interactions of water molecules with the surface of walls take place at 3.85 Å and hardly depend on temperature for both C14 and C10 samples. The structure of water in the monolayer sample for C14 does not change remarkably with temperature, consistent with no ice formation in the pores. The strong hydrogen-bonded interaction at the distance of 2.56 Å has been observed in the monolayer water.

Acknowledgment. This work has been partly supported by grants from the Ministry of Education, Science, Sports, and Culture of Japan (No. 08454227 and No. 0643060).

References and Notes

(1) Franks, F. *Water, A Comprehensive Treatise*; Plenum: New York, 1980; Vol. 7; Chapter 3 and the references therein.

(2) Clark, J. W.; Hall, P. G.; Piddack, A. J.; Wright, C. J. *J. Chem. Soc., Faraday Trans. 1* **1985**, *81*, 2067.

(3) Steytler, D. C.; Dore, J. C.; Wright, C. J. *J. Mol. Phys.* **1983**, *48*, 1031.

(4) Bellissent-Funel, M.-C.; Lal, J.; Bosio, L. *J. Chem. Phys.* **1993**, *98*, 4246.

(5) Bellissent-Funel, M.-C.; Bradley, K. F.; Chen, S. H.; Lai, J.; Teixeira, J. *Physica A* **1993**, *201*, 277.

(6) Takamuku, T.; Yamagami, M.; Wakita, H.; Masuda, Y.; Yamaguchi, T. *J. Phys. Chem. B* **1997**, *101*, 5730.

(7) Beck, J. S.; Vartulli, J. C.; Roth, W. J.; Leonowicz, M. E.; Kresger, C. T.; Schmitt, K. D.; Chu, C. T.-W.; Olson, D. H.; Sheppard, E. W.; McCullen, S. B.; Higgins, J. B.; Schlenker, J. L. *J. Am. Chem. Soc.* **1992**, *114*, 10933.

(8) Chen, C. Y.; Li, H. X.; Davis, M. *Mesoporous Mater* **1993**, *2*, 17.

(9) Hansen, E. W.; Stöcker, M.; Schmidt, R. *J. Phys. Chem.* **1996**, *100*, 2195.

(10) Morishige, K.; Nobuoka, K. *J. Chem. Phys.* **1997**, *107*, 6965.

(11) Takahara, S.; Nakano, M.; Kittaka, S.; Kuroda, Y.; Mori, T.; Hamano, H.; Yamaguchi, T. *J. Phys. Chem. B* **1999**, *103*, 5814.

(12) Dollimore, D.; Heal, G. G. R. *J. Appl. Chem.* **1964**, *14*, 199.

(13) Yamanaka, K.; Yamaguchi, T.; Wakita, H. *J. Chem. Phys.* **1994**, *101*, 9830.

(14) Yamaguchi, T.; Johansson, G.; Holmberg, B.; Maeda, M.; Ohtaki, H. *Acta Chem. Scand.* **1984**, *A38*, 437.

(15) Johansson, G.; Sandström, M. *Chem. Scr.* **1973**, *4*, 195.

(16) Narten, A. H.; Danford, M. D.; Levy, H. A. ORNL-3997, Oak Ridge National Laboratory: Oak Ridge, TN, 1966.

(17) Ohtaki, H.; Radnai, T.; Yamaguchi, T. *Chem. Soc. Rev.* **1997**, 41.

(18) Peterson, S. W.; Levy, H. A. *Acta Crystallogr.* **1957**, *10*, 70.

(19) Lee, S. H.; Rossky, P. J. *J. Chem. Phys.* **1994**, *100*, 3334.

(20) Yamaguchi, T. Doctoral Thesis, Tokyo Institute of Technology, 1978.

(21) Soper, A. K.; Bruni, F.; Ricci, M. A. *J. Chem. Phys.* **1998**, *109*, 1486.

(22) Okhulkov, A. V.; Damianets, Y. N.; Gorbaty, Y. E. *J. Chem. Phys.* **1994**, *100*, 1578.

(23) *Kyuchaku no Kagaku* (in Japanese) (*Science of Adsoprtion*); Kondo, S., Ishikawa, T., Abe, I., Eds.; Maruzen: Tokyo, 1991; p 205.

(24) Belfort, G.; Sinai, N. In *Water in Polymer*; Rowland, S. P., Ed.; ACS Symposium Series; American Chemical Society, Washington, DC, 1980; Vol. 127, p 323.

(25) Triolo, R.; Narten, A. H. *J. Chem. Phys.* **1975**, *63*, 3624.

(26) Lee, H.-G.; Matsumoto, Y.; Yamaguchi, T.; Ohtaki, H. *Bull. Chem. Soc. Jpn.* **1983**, *56*, 443.